

2. Glacial isostatic adjustment of Scandinavia and north-western Europe and the radial viscosity structure of the Earth's mantle

Abstract^a

During the last glacial maximum, large ice sheets covered Scandinavia, the Barents Sea, and the Northern British Isles. Subsequent to the last glacial maximum, the ice sheets disappeared and the solid Earth readjusts towards a new isostatic equilibrium. The glacial isostatic adjustment process is documented in numerous observations, e. g. palaeo-shorelines covering the last deglaciation phase, and ongoing crustal deformations monitored by GPS stations, e. g. the BIFROST project. In this study, we use palaeo-shoreline data from Scandinavia, the Barents Sea, and northwestern Europe as well as radial crustal velocities from the BIFROST campaign to infer the radial viscosity structure of the Earth's mantle underneath Scandinavia and northwestern Europe. A global inverse procedure based on the Neighbourhood Algorithm allows us to explore the hypothesis of a low-viscosity zone in the upper mantle, which has been proposed in the literature. Our results indicate a low-viscosity zone underneath the Barents Sea, with viscosities between 10^{19} - 10^{20} Pa s in a depth interval of 160 - 200 km. No such low-viscosity zone is found underneath Scandinavia, and no clear indication for such a zone underneath northwestern Europe. The thickness of the rheological lithosphere increases from 60 - 70 km underneath the northwestern Europe and the Barents Sea towards values exceeding 120 km underneath Scandinavia.

^aSteffen and Kaufmann (2006). Glacial isostatic adjustment of Scandinavia and north-western Europe and the radial viscosity structure of the Earth's mantle, *Geophys. J. Int.* 163/2, 801-812.

2.1 Introduction

During the Quaternary period, surface temperatures on the Earth have repeatedly dropped by more than 10°C. These palaeo-climatic variations have induced the growth of large ice sheets over North America and Europe. The interior of the Earth has responded to the additional weight of these palaeo-ice sheets by adjusting its shape: During the build-up of ice sheets the surface was depressed by several hundreds of metres, during the melting phase the surface rebounded to its initial state. The viscoelastic nature of this process, termed *glacial isostatic adjustment* (GIA), causes a time delay between the removal of the last palaeo-ice sheets and the deformation of the solid surface.

In Scandinavia and northwestern (NW) Europe, where the large Weichselian Ice Sheet complex was located during the last glacial cycle, the GIA process was recognised early as being responsible for numerous field observations [see Ekman, 1991, for a review]. The good geological record of the crustal response in Scandinavia, documented in various observations such as palaeo-shorelines (relative sea levels, RSL), shoreline tilting, and the present-day crustal motion, together with a reasonable knowledge of the ice-sheet retreat since the *last glacial maximum* (LGM), allow to construct a detailed model of sea-level change induced by the mass redistribution between ice sheets and the ocean.

In the past decade, numerical models of the GIA based on Scandinavian and NW European observational data have converged towards a radial viscosity structure, with viscosities increasing by one to two orders of magnitude with depth. The use of linear rheological laws for the Earth's mantle has been shown to be both an adequate and consistent description for deformations on the time scale of 10^2 to 10^7 years. Some representative examples for the interpretation of observational data for the Scandinavian and NW European regions will be discussed below.

Palaeo-shoreline data: Based on palaeo-shoreline data from the British Isles, Lambeck [1993a,b] has derived a simple radial viscosity profile, with viscosities increasing from $(4 - 5) \times 10^{20}$ Pa s in the upper mantle to 10^{22} Pa s in the lower mantle. Lambeck et al. [1996] have extended the interpretation of the British Isles data and concluded that the upper-mantle viscosity can be refined further, with viscosities ranging from 10^{20} Pa s for the low-velocity zone beneath the lithosphere to 10^{21} Pa s in the transition zone. In these studies, the lithospheric thickness best fitting the observations was around 70 km.

Using observational data from Northern Europe, Lambeck et al. [1998a] found a similar best-fitting viscosity structure, with lithospheric thickness values around 70 - 80 km, an upper-mantle viscosity around $(3 - 4) \times 10^{20}$ Pa s, and lower-mantle viscosity at least one order of magnitude larger.

Kaufmann and Lambeck [2002] improved mantle viscosity inferences for this region through the application of a formal inverse procedure to data sets of palaeo-shorelines, present-day sea level and crustal response, and rotational data. The mantle viscosity profiles found are characterised by a two order of magnitude variation with depth. Upper-mantle viscosity increases from 2×10^{20} below the lithosphere to around 10^{21} Pa s towards the 660-km seismic discontinuity. The rebound-related observations cannot distinguish between a sharp increase of viscosity between the upper and lower mantle, or a more gradual variation. The viscosity in the lower mantle is generally one order of magnitude larger, with peak values close to 10^{23} Pa s in around 1000 km depth.

Relaxation-time spectra: If high-quality palaeo-shoreline data exist – as in Scandinavia – spatially continuous palaeo-shoreline profiles may be constructed and an inverse relaxation-time spectrum (IRTS) be derived. The IRTS is based on the assumption of a free relaxation of the surface after the deglaciation event was completed. Using such a dataset, Wiczerkowski et al. [1999] inferred an average viscosity of the upper mantle beneath central Scandinavia of 5×10^{20} Pa s (between 95 and 515 km depth). The permitted lithospheric thickness values range between 70 and 120 km. Fleming et al. [2003] extended this interpretation by allowing the lithosphere to be viscoelastic, but they obtained similar viscosities for the upper mantle. Klemann and Wolf [2005] added two new shoreline diagrams to the dataset and obtained an upper-mantle viscosity of 5×10^{20} Pa s and a – poorly resolved – lower-mantle viscosity of 2.4×10^{21} Pa s.

Present-day crustal motions: The ongoing improvement of space-geodetic observations such as the global positioning system (GPS) allows a fairly accurate measurement of present-day crustal motions. The BIFROST project [Johansson et al., 2002] has recorded the three-dimensional crustal motion of Scandinavia over a period of seven years. Based on this dataset, Milne et al. [2001, 2004] have derived

a radial viscosity profile with permitted lithospheric thickness values between 90 and 170 km, upper-mantle viscosities in the range of $(5 - 10) \times 10^{20}$ Pa s, and lower-mantle viscosities in the range of $(0.5 - 5) \times 10^{22}$ Pa s.

Low-viscosity asthenosphere: In all of the examples quoted above, no particular attempt was made to resolve a *low-viscosity asthenosphere* underneath the elastic lithosphere. While the simple three-layer viscosity models [e.g. Lambeck, 1993a,b; Lambeck et al., 1998a; Wiczerkowski et al., 1999; Fleming et al., 2003] did not account for such a possibility, the more detailed viscosity profiles resulting from formal inverse procedures [e.g. Kaufmann and Lambeck, 2002; Milne et al., 2004] also found no evidence for a low-viscosity asthenosphere. There are, however, a number of publications, which have modelled the GIA of Scandinavia (mostly with flat geometries), and which favour a viscosity profile including a low-viscosity asthenosphere. Early results on the *asthenosphere problem* include a 100 km thick asthenosphere with 1.3×10^{19} Pa s [van Bemmelen and Berlage, 1935], a 200 km thick asthenosphere with 10^{20} Pa s [McConnell, 1968], a 75 km thick asthenosphere with 4×10^{19} Pa s [Cathles, 1975], and a 100 km thick asthenosphere with 1.2×10^{19} Pa s [Wolf, 1987]. Later on, Fjeldskaar [1994, 1997] used both present-day crustal motion data and palaeo-shoreline data from the Scandinavian region to infer the rheological layering of the Earth's mantle, using a GIA model. He strongly advocated the presence of a low-viscosity asthenosphere, at most 150 km thick and with a viscosity around 7×10^{19} Pa s.

Further evidence of a weak asthenospheric layer offshore Western Europe comes from seismic tomographical imaging [e.g. Su and Dziewonski, 1991; Li and Romanowicz, 1996; Romanowicz, 1998; Ekström and Dziewonski, 1998]. Here, the shear-wave velocity anomalies underneath the Atlantic and western Scandinavia indicate lower than average velocities underneath the ocean, while central Scandinavia is characterised by higher than average shear-wave velocities [Ekström and Dziewonski, 1998]. Relating the shear-wave velocity perturbations to density variations, which in turn are (at least partially) related to temperature variations [e.g. Ivins and Sammis, 1995], the seismic velocities down to 400 km depth clearly reveal the cold, more viscous mantle material of the Baltic Shield, and a warmer, less viscous region offshore the Scandinavian West Coast, possibly correlated to the Mid-Atlantic Ridge.

The effect of such a three-dimensional viscosity structure on models of GIA has been discussed in the literature [e.g. Kaufmann and Lambeck, 2000; Kaufmann and Wu, 2002]. It has been shown that lateral variations in lithospheric thickness and in asthenospheric viscosity do influence model predictions of palaeo-shorelines and crustal motions. However, Martinec and Wolf [2005] have shown that a two-dimensional earth model for Scandinavia with a central 200 km thick lithosphere underneath the Gulf of Bothnia and a peripheral 80 km thick lithosphere underlain by a 100 km thick asthenosphere with 8×10^{18} Pa s essentially results in the same IRTS for central Scandinavia as a one-dimensional viscosity profile with a 100 km thick lithosphere and no asthenosphere. Hence, they found no strong evidence for a weak asthenosphere.

In this paper we return to the question of a weak asthenosphere underneath Scandinavia and NW Europe. Therefore sea-level data from Scandinavia, the Barents Sea, the North Sea, the British Isles and the Atlantic and English Channel coasts were collected. The global ice model RSES (developed by Kurt Lambeck from the Research School of Earth Sciences, Canberra, Australia) was used to predict GIA and then predictions are compared to the observed data. For the subregions Scandinavia, NW Europe, and the Barents Sea, we determine the best simple (three-layer) viscosity profile for each region, then a global inverse procedure is employed to further refine the viscosity profile in the upper mantle.

2.2 Theory

The results presented in this paper are based on model predictions for a spherically symmetric, compressible, Maxwell-viscoelastic earth model. The elastic structure is derived from PREM [Dziewonski and Anderson, 1981], and lithospheric thickness is a free parameter. Mantle viscosity is parameterised in several sub-lithospheric layers with constant viscosity within each layer. The Earth's core is assumed to be inviscid, and incorporated as lower boundary condition.

We solve the sea-level equation [Farrell and Clark, 1976] for a rotating Earth given by

$$W(\theta, \varphi, t) = C(\theta, \varphi, t) [G(\theta, \varphi, t) - R(\theta, \varphi, t)]. \quad (2.1)$$

In (2.1), θ and φ are co-latitude and eastern longitude, t is time, $W(\theta, \varphi, t)$ is the ocean load thickness, $G(\theta, \varphi, t)$ and $R(\theta, \varphi, t)$ are response functions of the geoidal and the radial surface displacements [for details see Kaufmann and Lambeck, 2002], and $C(\theta, \varphi, t)$ is the time-dependent ocean function [Munk and MacDonald, 1960], equalling one over oceanic areas and zero elsewhere. The sea-level equation can be rewritten as an integral equation, which we solve iteratively. Once we have determined the ocean load thickness W , we derive several quantities of interest, such as relative sea-level change, present-day surface motions, time-dependent perturbations of the gravitational field, and rotational contributions from the ice-ocean imbalance. We follow the pseudo-spectral approach outlined in Mitrovica et al. [1994] and Mitrovica and Milne [1998], using an iterative procedure in the spectral domain, and a spherical harmonic expansion truncated at degree 192. The calculated quantities are then compared to observational data.

2.3 Ice and ocean models

The surface load comprises two contributions: The Late Pleistocene ice sheet thickness, $I(\theta, \varphi, t)$, and the corresponding ocean load thickness, $W(\theta, \varphi, t)$. Introducing the densities of ice and water, ρ_I and ρ_W , we find the surface load density:

$$L(\theta, \varphi, t) = \rho_I I(\theta, \varphi, t) + \rho_W W(\theta, \varphi, t). \quad (2.2)$$

For the Late Pleistocene glacial history, the ice model RSES is used. RSES is a global ice model comprising Late Pleistocene ice sheets over North America, North Europe, Greenland, the British Isles, and Antarctica. The extent and the melting history follow model ICE-1 [Peltier and Andrews, 1976] for the Laurentide Ice Sheet and Greenland, model FBKS8 [Lambeck et al., 1998a] for the Scandinavian and Barents Sea Ice Sheets, model BK4 [Lambeck, 1993b] for the British Ice Sheet, and model ANT3 [Nakada and Lambeck, 1988] for the Antarctic Ice Sheet. All reconstructions are based on glaciological and geomorphological evidence and thus reflect the approximate extent of the Late Pleistocene Ice Sheets throughout the last glacial cycle. Of these ice sheets only the Scandinavian, Barents Sea and British Isles ice sheets are high spatial and temporal resolution models that are consistent with the majority of the field evidence for ice-margin retreat and with the rebound data. The Antarctic and Laurentide ice sheets are both of a coarser resolution, which, however, is of secondary importance for our regional study. All ice sheet models have been converted from the radiocarbon timescale to the U/Th timescale, using the CALIB-4 program [Stuiver and Reimer, 1993; Stuiver et al., 1998]. The ice volume at the LGM approximately 21,400 years BP corresponds to 124 m of eustatic sea-level change, and the extent for four different times is shown in Fig. 2.1. We simulate the time-dependence of the ice sheets throughout the Late Pleistocene glacial cycles by modelling the last two cycles with linear changes in ice load thickness

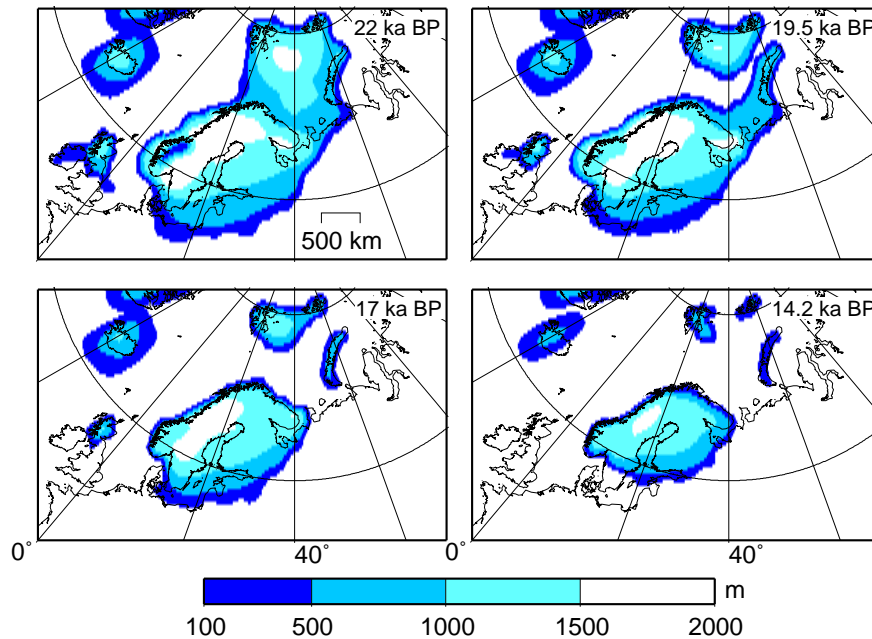


Figure 2.1: Map of ice model RSES over Europe for four different time epochs. Contours are drawn every 500 m.

approximating the oxygen isotope data record [Chappell and Shackleton, 1986] and by assuming a time-averaged ice load before that time. This parameterisation of the last glacial cycles has been shown to be sufficient to correctly predict changes in the Earth's gravitational field and rotation, as well as surface displacements [Johnston and Lambeck, 1999]. For the deglaciation following the LGM, the more detailed ice load thickness maps are used.

2.4 Observational data

For our analysis, we have chosen observed sea-level indicators from Scandinavia (569), the Barents Sea (264), and NW Europe (487) sampling the near field of the Weichselian Ice Sheet fairly evenly (Fig. 2.2). The Barents Sea data (circles) are based on several studies and were summarised in Kaufmann and Wolf [1996]. NW Europe data (squares) are taken from Lambeck [1993a,b]. The Scandinavian observations (triangles for central locations and inverse triangles for peripheral locations) are summarised in Lambeck et al. [1998a]. The data are based on faunal assemblages and preservation status of sediments. Radiocarbon dating was used and converted to U/Th-times.

The RSL data reflect the complicated three-dimensional response of the solid Earth to changes in the ice and ocean load and thus are reliable constraints for mantle viscosity models. The spatial and temporal distribution of the RSL data can be seen in Fig. 2.3: The Scandinavian RSL data cover a broad range from present-day sea level to more than 250 m height, while reaching back to around 15,000 years, with isolated data even marking the LGM. The deformation process of the solid Earth is therefore documented over a wide spatio-temporal range. The NW Europe RSL data are much smaller in amplitude, reaching only heights around 60 m. A significant part of the data is submerged down to 50 m depth, documenting a significant contribution from sea-level rise. The temporal distribution covers the last 18,000 years. The

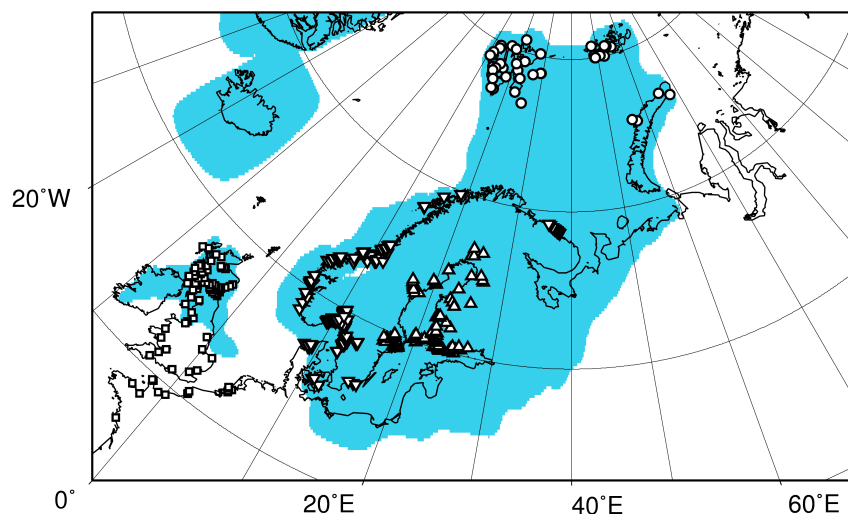


Figure 2.2: Map of Europe, with ice margins at last glacial maximum superimposed in blue. Locations for RSL data are shown as symbols for Scandinavia (569 triangles, triangles for central, inverted triangles for peripheral regions), the Barents Sea (264 circles), and the NW Europe (487 squares).

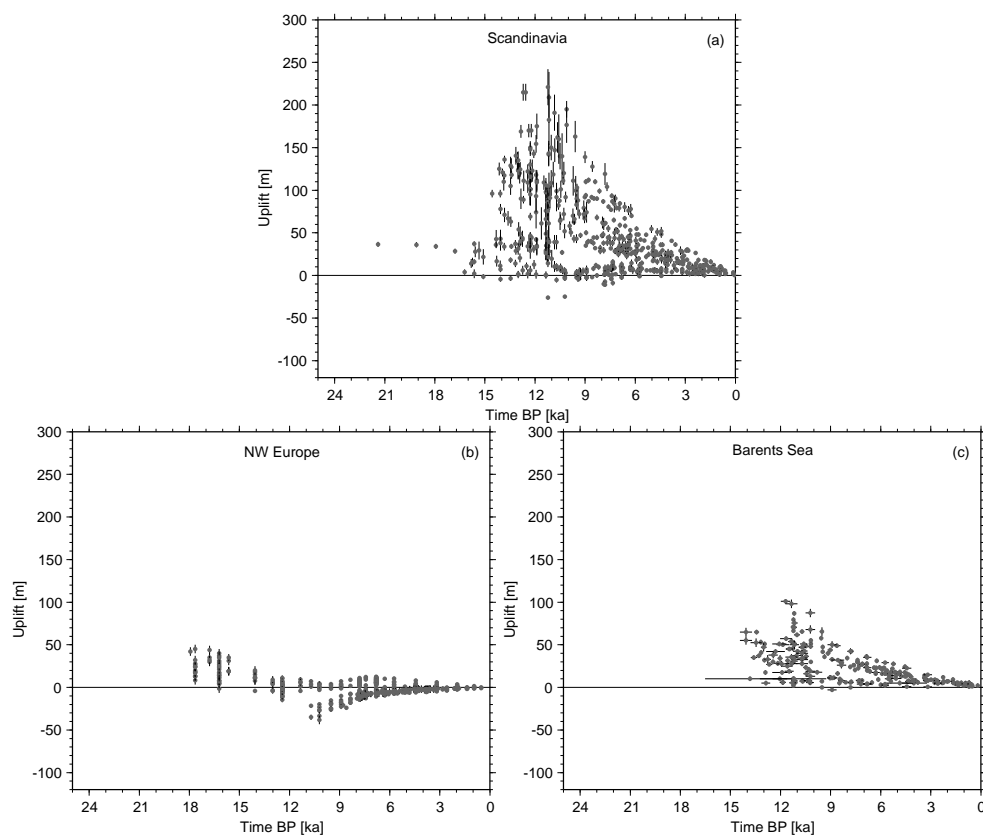


Figure 2.3: Summary of RSL datasets. Dots are observations, bars the uncertainties of the data. (a) Scandinavian RSL data, (b) NW European RSL data, (c) Barents Sea RSL data.

Barents Sea RSL data are restricted to land uplift, with amplitudes up to 120 m. However, the temporal distribution is more limited, reaching 14,000 years back in time.

In addition to the sea-level indicators we use the vertical velocities determined by the BIFROST project [Johansson et al., 2002].

2.5 Results

In this section, we present model predictions of RSL changes and we compare the predictions to the three subsets of RSL data from Scandinavia, NW Europe, and the Barents Sea. The comparison of model predictions and data is based on a least-squares misfit, defined as

$$\chi = \sqrt{\frac{1}{n} \sum_{i=1}^n \left(\frac{o_i - p_i(a_j)}{\Delta o_i} \right)^2}, \quad (2.3)$$

with n the number of observations considered, o_i the observed RSL or BIFROST data, $p_i(a_j)$ the predicted RSL for a specific earth model a_j , and Δo_i the data uncertainties. We search for the minimum value of χ within the parameter range, which gives us an earth model a_b , fitting the observational dataset best. If the model is complete and the observational uncertainties are normally distributed with known standard deviations and uncorrelated, the expected best fit would be $\chi = 1$. To bracket all earth models, which fit the observational data equally well as the best-fitting earth model a_b within the observational uncertainties, a confidence parameter is calculated:

$$\Psi = \sqrt{\frac{1}{n} \sum_{i=1}^n \left(\frac{p_i(a_b) - p_i(a_j)}{\Delta o_i} \right)^2}. \quad (2.4)$$

For all confidence parameters $\Psi \leq 1$, the prediction $p_i(a_j)$ fits the data as well as the best-fitting model $p_i(a_b)$ within the 1σ -uncertainty.

2.5.1 Three-layer models

We start discussing our results with a parameter search through the three-dimensional parameter space lithospheric thickness H_l , upper-mantle viscosity η_{UM} , lower-mantle viscosity η_{LM} for the three-layer earth models. Elastic parameters are assigned from PREM [Dziewonski and Anderson, 1981], and the parameter space of the free parameters is listed in Tab. 2.1. The total number of earth models calculated is 1089.

Scandinavia: In Fig. 2.4a and b, the misfit values based on the Scandinavian RSL data are shown as misfit maps of the parameter space. The best-fitting three-layer earth model found has a fairly thick lithosphere of $H_l = 120$ km, an upper-mantle viscosity of $\eta_{UM} = 4 \times 10^{20}$ Pa s, and a lower-mantle viscosity of $\eta_{LM} = 10^{23}$ Pa s. The misfit for this model is $\chi = 2.71$. While the upper-mantle viscosity is well constrained ($\eta_{UM} \in [3, 5] \times 10^{20}$ Pa s), the predictions are largely insensitive to the lithospheric thickness over a large range of parameter values ($H_l \in [100, 140]$ km), as it can be seen by the large confidence regions in Fig. 2.4a. Similarly, the RSL data from Scandinavia are not very sensitive to lower-mantle viscosity, as the confidence region in Fig. 2.4b covers a range from $\eta_{LM} \in [3 \times 10^{22}, 10^{23}]$ Pa s. The estimate of the upper-mantle viscosity found agrees with previous studies, e.g. the inference from Lambeck et al. [1998a,b] of $\eta_{UM} = 4 \times 10^{20}$ Pa s based on Scandinavian RSL data, the $\eta_{UM} = 5 \times$

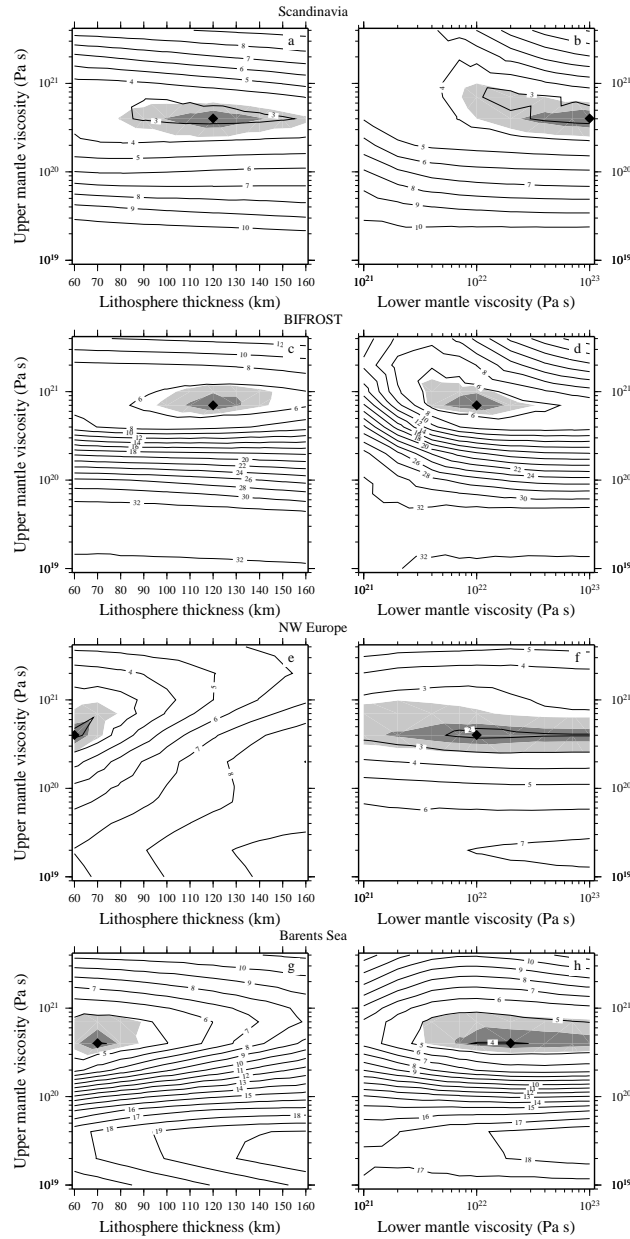


Figure 2.4: Misfit for ice model RSES, three-layer earth model and different data sets: (a) Misfit map for Scandinavian RSL data as a function of lithospheric thickness and upper-mantle viscosity for a fixed lower-mantle viscosity of 10^{23} Pa s. (b) Misfit map for Scandinavian RSL data as a function of upper and lower-mantle viscosities for a fixed lithospheric thickness of 120 km. (c) Misfit map for the BIFROST data as a function of lithospheric thickness and upper-mantle viscosity for a fixed lower-mantle viscosity of 10^{22} Pa s. (d) Misfit map for the BIFROST data as a function of upper and lower-mantle viscosities for a fixed lithospheric thickness of 120 km. (e) Misfit map for the NW European RSL data as a function of lithospheric thickness and upper-mantle viscosity for a fixed lower-mantle viscosity of 10^{22} Pa s. (f) Misfit map for the NW European RSL data as a function of upper and lower-mantle viscosities for a fixed lithospheric thickness of 60 km. (g) Misfit map for the Barents Sea RSL data as a function of lithospheric thickness and upper-mantle viscosity for a fixed lower-mantle viscosity of 2×10^{22} Pa s. (h) Misfit map for the Barents Sea RSL data as a function of upper and lower-mantle viscosities for a fixed lithospheric thickness of 70 km. The best 3-layer earth model is marked with a diamond, the light and dark shadings indicate the confidence regions $\Psi \leq 1$ and $1 < \Psi \leq 2$, respectively.

10^{20} Pa s estimate from Wiczerkowski et al. [1999] and Klemann and Wolf [2005] based on the IRTS of Scandinavia, the value of $\eta_{UM} \in [5 \times 10^{20}, 10^{21}]$ Pa s from Milne et al. [2004], based on the BIFROST crustal motion data, and the results from Martinec and Wolf [2005] in the range of $(4 - 6) \times 10^{20}$ Pa s based on the IRTS including a lithospheric root. The estimate for the lithospheric thickness is at the upper limit of previous estimates, but viewed in the light of the larger permitted range of lithospheric thickness values, the best model is satisfactory. The low resolving power for lower-mantle viscosity also agrees well with the estimated depth resolution of the Scandinavian RSL data, which according to Mitrović [1996] is limited to the upper 1000 - 1400 km of the Earth's mantle.

We have subdivided the Scandinavian RSL dataset further into *central* locations close to the former ice sheet centre (triangles in Fig. 2.2), and *peripheral* locations around the coastal areas (inverted triangles in Fig. 2.2). With this subdivision we have tested for different best lithospheric thickness estimates in these different regions. As it can be seen in Tab. 2.1, the RSL data from the central region prefer a thick lithosphere ($H_l = 160$ km), while the peripheral RSL data result in a thinner lithosphere ($H_l = 100$ km). The different lithospheric thickness estimates correlate with the seismic observation of a thick cratonic root underneath central Scandinavia [e.g. Panza et al., 1980; Calcagnile, 1982; Goes and Govers, 2000]. The permitted ranges for the lithospheric thickness values, $H_l \in [140, 160]$ km for the central and $H_l \in [80, 120]$ km for the peripheral regions, indicate that the distinction of different lithospheric thickness estimates is significant.

In Fig. 2.4c and d, the misfit values based on the data of vertical crustal motion of Scandinavia (BIFROST project) are shown. The best-fitting three-layer earth model found has a lithospheric thickness of $H_l = 120$ km, and upper- and lower-mantle viscosities of $\eta_{UM} = 7 \times 10^{20}$ Pa s and $\eta_{LM} = 1 \times 10^{22}$ Pa s, respectively. The misfit for this model is $\chi = 4.59$. The upper mantle is well constrained ($\eta_{UM} \in [6, 9] \times 10^{20}$ Pa s), while the lithosphere in Fig. 2.4c can be predicted within a tight range of parameter values ($H_l \in [110, 130]$ km). The lower mantle confidence region in Fig. 2.4d covers a range from $\eta_{LM} \in [5 \times 10^{21}, 2 \times 10^{22}]$ Pa s. These values agree well with the earlier results of Milne et al. [2001, 2004]. We have not subdivided the BIFROST data into central and peripheral locations, as there are practically no data along the periphery (Norwegian Coast).

NW Europe: In Fig. 2.4e and f, the misfit values based on the British Isles and Central European RSL data are shown. The best-fitting three-layer earth model for this data subset is characterised by a lithospheric thickness of $H_l = 60$ km, and upper- and lower-mantle viscosities of $\eta_{UM} = 4 \times 10^{20}$ and $\eta_{LM} = 10^{22}$ Pa s, respectively. The misfit for this model is $\chi = 1.81$. All values agree well with the earlier inference of the British Isles RSL data from Lambeck [1993a,b]. While the large confidence range for the lower-mantle viscosity ($\eta_{LM} \in [2 \times 10^{21}, 10^{23}]$ Pa s) again confirms the poor resolving power of the NW European RSL data for larger mantle depths, the lithospheric thickness is better constrained, with permissible ranges limited to $H_l \in [60, 70]$ km.

Barents Sea: In Fig. 2.4g and h, the misfit values based on the Barents Sea palaeo-shoreline data are shown. The best-fitting three-layer earth model for this data subset is characterised by a lithospheric thickness of $H_l = 70$ km, and upper- and lower-mantle viscosities of $\eta_{UM} = 4 \times 10^{20}$ and $\eta_{LM} = 2 \times 10^{22}$ Pa s, respectively. However, the misfit for this model is $\chi = 3.96$, which is significantly worse than for the previous datasets for Scandinavia and the British Isles. This might be a result of the less reliable ice-sheet reconstruction over this region, or of an inadequate earth model. Again, lower-mantle viscosity is almost unconstrained, while the range of permitted lithospheric thickness values is $H_l \in [65, 75]$ km.

Tab. 2.1 summarises the results discussed above. Here, upper-mantle viscosities for all regions are around 4×10^{20} Pa s, and cover a range between $\eta_{UM} \in [3 \times 10^{20}, 5 \times 10^{20}]$ Pa s. Compared to the results of Kaufmann & Amelung [2000] with upper-mantle viscosities of $(2 - 5) \times 10^{20}$ Pa s, we find a good

Table 2.1: Three-layer earth models. Free parameters are lithospheric thickness H_l , upper-mantle viscosity η_{UM} , lower-mantle viscosity η_{LM} . χ_{three} is the misfit for the best 3-layer earth model. Results for the three-layer earth models fitting the data within the 1σ -uncertainty range are shown for the different data sets, with the best-fitting earth model in brackets.

	H_l km	η_{UM} 10^{20} Pa s	η_{LM} 10^{22} Pa s	χ_{three}
Search range	60-160	0.1-40	0.1-10	
Dataset	RSES			
Scandinavia	100-140 (120)	3-5 (4)	3-10 (10)	2.71
central	140-160 (160)	3-5 (4)	2-10 (10)	1.94
peripheral	80-120 (100)	5-10 (7)	2-10 (7)	2.60
NW Europe	60-70 (60)	3-6 (4)	0.2-10 (1)	1.81
Barents Sea	65-75 (70)	3-6 (4)	0.7-10 (2)	3.96
BIFROST	110-130 (120)	6-9 (7)	0.5-2 (1)	4.59

agreement. The lower-mantle viscosity is almost unconstrained, confirming the low resolving power for lower-mantle viscosity of the Scandinavian RSL data [see Mitrovia, 1996, for more information]. The thickness of the lithosphere indicates a lithospheric root (160 km thick) under the Archean crust of Scandinavia, decreasing towards the Mid Ocean Ridges in the Atlantic and Arctic Ocean. Here, the lithosphere has a thickness of 60 km under the British Isles and 70 km under the Barents Sea.

2.5.2 Multi-layer models

Next, we try to assess the potential of the datasets to resolve more structure in the Earth's mantle. Our aim is to search for a possible low-viscosity zone in the uppermost mantle, as proposed, for example, by Fjeldskaar [1994, 1997] for the Scandinavian region. Therefore, we refine our radial viscosity structure in the upper mantle as follows: We first assign a thickness of 60 km for the first layer, representing the elastic lithosphere, which is in agreement with the results for the NW European and Barents Sea RSL data. The rest of the upper mantle is subdivided into five layers with viscosities $\eta_{UMi}, i = 1, 5$. The thickness values of these layers are: $H_{UM1} = 60$ km, $H_{UM2} = 40$ km, $H_{UM3} = 40$ km, $H_{UM4} = 230$ km, $H_{UM5} = 230$ km. The lower mantle remains uniform, stretching from the 660 km seismic discontinuity to the core-mantle boundary, with a viscosity fixed to the best-fitting result from the three-layer model for each data set. This choice of refinement is guided by the three-layer earth models, which have shown the poor resolving power of the RSL data for lower-mantle structure.

Simple forward search in the parameter space, as done in the three-layer earth model cases, is no longer suitable for the proposed multi-layer earth models. In the past, more detailed radial viscosity structures derived from GIA-related observations have been performed by formal inverse procedures, such as Tarantola-Valette inverse procedures [e. g. Kaufmann and Lambeck, 2002] or Bayesian inverse procedures [e. g. Forte and Mitrovia, 1996; Mitrovia and Forte, 1997; Peltier, 1998; Milne et al., 2004]. These methods are all based on a linearisation of the non-linear inverse problem of mantle viscosity, and thus depend on an a-priori viscosity profile as a starting model. Usually, such an a-priori profile was based on a simpler three-layer earth model. However, the resulting inverse inference of the more detailed viscosity profile, though having a more detailed depth resolution, critically depends on the a priori starting model [see Kaufmann and Lambeck, 2002, for a detailed investigation of this dependence].

In this paper, we have chosen a different approach, using a global-search inverse procedure based on the Neighbourhood Algorithm (NA). The Neighbourhood algorithm introduced by Sambridge [1999a,b] is a direct search method for non-linear inverse problems. The NA method is applicable to a wide range of inversion problems, particularly those with rather complex dependencies between data and model. During the search stage of the NA method, a multidimensional parameter space is sampled for combinations of model parameters, which provide a satisfactory fit to the observed data. The search is guided by randomised decisions similar to techniques used for genetic algorithms (GA) and simulated annealing (SA), but the NA method needs only two control parameters. A misfit between model prediction and observation is calculated, and the search is driven towards the minimum misfit within the parameter space. The NA method is based on the geometrical concept of Voronoi cells. These Voronoi cells are nearest-neighbour regions around each sampling point. The Voronoi cells are used to guide the sampling. Further details can be found in Sambridge [1998, 2001].

The NA method is run in several steps:

1. We initialise the NA search for one RSL dataset o_i with an initial set of $n_{si} = 1000$ models, generated randomly within the 5D parameter space of upper-mantle viscosities. The search range for all upper-mantle viscosity layers is $\eta_{UM1} - \eta_{UM5} \in [10^{19}, 10^{22}]$ Pa s. For each of these n_{si} forward models, the misfit function (2.3) is then calculated.
2. We then use the $n_r = 10$ best-fitting models of the initial ensemble, define Voronoi cells around each of the n_r samples, and place $n_s = 20$ new models within these n_r cells (that is n_s/n_r new models in each cell).
3. For the n_s new models, the misfit function is evaluated, and the algorithm returns to step 2. Steps 2 and 3 are repeated $N = 25$ times, resulting in a total of $n_{si} + N \times n_s = 1500$ model predictions for each data set.

An example of the misfit reduction is shown in Fig. 2.5. Here, the $n_{si} = 1000$ initial samples result in a misfit around $\chi \sim 8$. Then, the NA method starts refining the regions of lowest misfit, and misfit values drop significantly over the next N iterations. The rough misfit curve indicates the resampling of the $n_r = 10$ best cells at a given iteration step, hence in between misfits might increase, but then the NA method leaves this local minimum in misfit, and continues to trace the best global minimum within the parameter range.

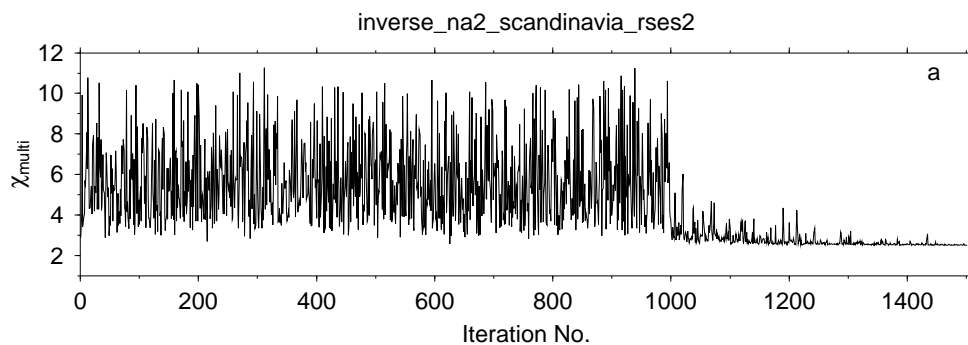


Figure 2.5: Misfit χ_{multi} as a function of the iteration counter.

In Fig. 2.6a, the best-fitting multi-layer viscosity profile based on the Scandinavian RSL dataset is shown as black line. Also shown as grey lines are all multi-layer viscosity profiles, which fit the RSL data equally well within the 1σ -uncertainty, based on the confidence parameter (2.4). Misfit values have dropped from an initial value of $\chi_{three} = 2.71$ to a final value of $\chi_{multi} = 2.51$, an improvement of only 8 percent. Two points are obvious: Firstly, the relatively high viscosity in the first layer ($\eta_{UM1} \in [2 \times 10^{21}, 10^{22}]$ Pa s) tries to rebuild the lower part of the elastic lithosphere, which was found previously by the three-layer model. Secondly, viscosities in the other four layers are only determined to within half to one order of magnitude. For the second and third layer, the possible asthenosphere, valid viscosities are $\eta_{UM2} \in [1 \times 10^{20}, 4 \times 10^{21}]$ Pa s and $\eta_{UM3} \in [8 \times 10^{19}, 2 \times 10^{21}]$ Pa s. Thus, no indication for a low-viscosity asthenosphere is found. For the two lowermost layers, permitted viscosities are $\eta_{UM4} \in [5 \times 10^{19}, 2 \times 10^{20}]$ Pa s and $\eta_{UM5} \in [2 \times 10^{21}, 1 \times 10^{22}]$ Pa s. Hence, only the fourth layer, below a depth of 200 km, is characterised by a viscosity around 10^{20} Pa s.

We also performed a NA inversion for the BIFROST uplift data. In Fig. 2.6b, the best-fitting multi-layer viscosity profile based on the BIFROST dataset is shown as black line. Here, the misfit is reduced by 12 percent from $\chi_{three} = 4.59$ to $\chi_{multi} = 4.06$. Both viscosities in the first and second layer are acceptable to within one order of magnitude: $\eta_{UM1} \in [2 \times 10^{19}, 4 \times 10^{20}]$ Pa s and $\eta_{UM2} \in [2 \times 10^{19}, 2 \times 10^{20}]$ Pa s. Interestingly, the best-fitting viscosity profile from the BIFROST data indicates a fairly low-viscosity of 2×10^{19} Pa s in the region between 160 and 200 km depth. However, acceptable viscosities for this depth range spread over a large range: $\eta_{UM3} \in [1 \times 10^{19}, 1 \times 10^{22}]$ Pa s. A similar feature has also been found by Milne et al. [2004] in their Bayesian inversion, and the authors also claim that their thin low-viscosity zone is also not resolvable by the BIFROST data. In the remaining upper mantle, the viscosity profile is not too different from the one found from the Scandinavian RSL data (Fig. 2.6a).

In Fig. 2.6c, the best-fitting multi-layer viscosity profile based on the NW European RSL dataset is shown as black line. Misfit values have dropped from an initial value of $\chi_{three} = 1.81$ to a final value of $\chi_{multi} = 1.60$, an improvement of around 12 percent. However, the permitted viscosity profiles vary over a large range throughout the entire upper mantle (see Tab. 2.2), indicating the poor resolving power of the NW European RSL data for more structure in the upper mantle. In a further test, we have excluded most of the submerged RSL data points from the NW European dataset, as they are dominated by the signal of sea-level rise. However, searching the 5D-parameter space of upper-mantle viscosities for the reduced dataset results in an almost identical set of viscosity profiles as shown in Fig. 2.6c. Thus we argue that the small spatial amplitudes of the NW European RSL data as shown in Fig. 2.3b do not provide more detailed information of the upper mantle viscosity structure.

In Fig. 2.6e, the best-fitting multi-layer viscosity profile based on the Barents Sea RSL dataset is shown as black line. Misfit values have dropped from an initial value of $\chi_{three} = 3.96$ to a final value of $\chi_{multi} = 2.68$, an improvement of more than 32 percent. Here, viscosities between 120 and 200 km depth indicate a low-viscosity asthenosphere, with viscosities of $\eta_{UM2} \in [1 \times 10^{19}, 1 \times 10^{20}]$ Pa s and $\eta_{UM3} \in [1 \times 10^{19}, 1 \times 10^{20}]$ Pa s. However, the inversion provides an alternative viscosity profile with a low viscosity of $\eta_{UM1} = 3 \times 10^{19}$ Pa s directly beneath the 60 km thick lithosphere and a high viscosity of $\eta_{UM2} = 6 \times 10^{21}$ Pa s in the layer below. Thus, the location of the low-viscosity asthenosphere is not well determined. Below a depth of 200 km, viscosities are again similar to the inference based on the Scandinavian RSL data.

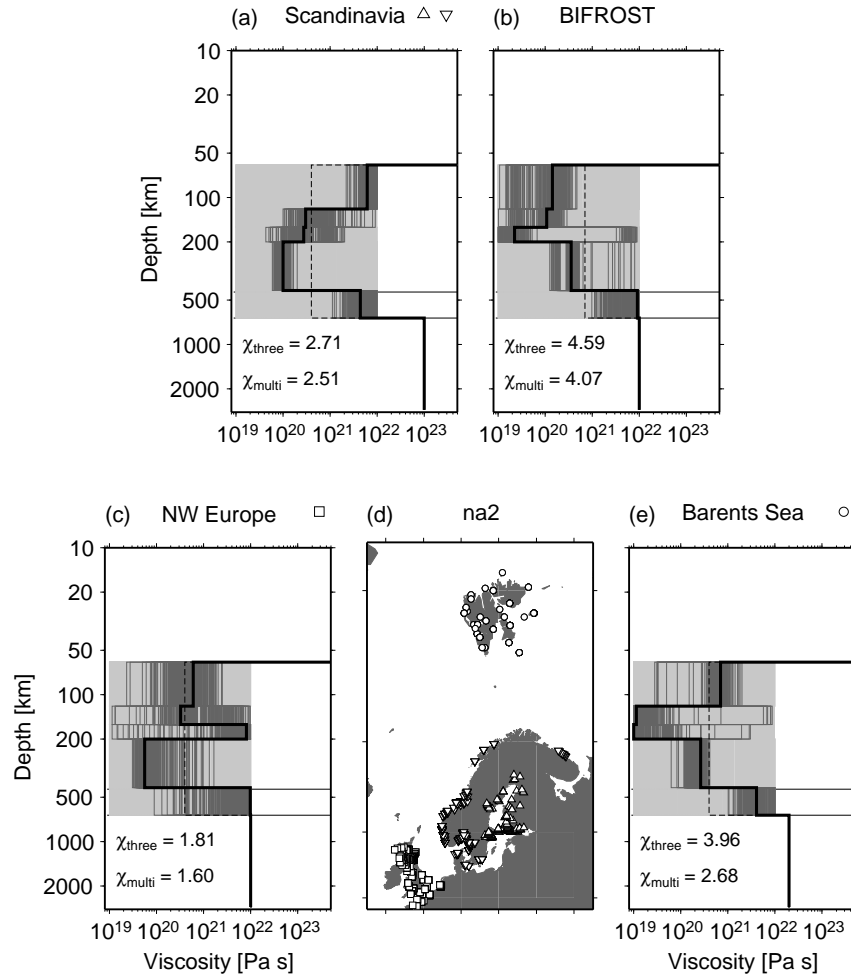


Figure 2.6: Best earth models from NA inversion for (a) the Scandinavian RSL data, (b) the BIFROST uplift data, (c) the NW European RSL data, and (e) the Barents Sea RSL data. RSL locations are marked by symbols and shown in the map (d). Shown are the best 3-layer viscosity profile (dashed line), the search range for all multi-layer viscosity profiles (light grey area), all multi-layer viscosity profiles acceptable within the 1σ -uncertainty range (dark grey lines), and the best multi-layer viscosity profile (solid line).

Table 2.2: Multi-layer earth models. Fixed parameters are lithospheric thickness ($H_l = 60$ km) and lower-mantle viscosity (η_{LM} , fixed to best three-layer inference). Free parameters are the upper-mantle viscosities $\eta_{UMi}, i = 1, 5$. χ_{multi} is the misfit for the best multi-layer earth model. Results for the multi-layer earth models fitting the data within the 1σ -uncertainty range are shown for the different data sets, with the best-fitting earth model in brackets.

	η_{UM1} 10^{20} Pa s	η_{UM2} 10^{20} Pa s	η_{UM3} 10^{20} Pa s	η_{UM4} 10^{20} Pa s	η_{UM5} 10^{20} Pa s	χ_{multi}
Search range	0.1-100	0.1-100	0.1-100	0.1-100	0.1-100	
Dataset	RSES					
Scandinavia	20-100 (60)	1-40 (3)	0.8-20 (3)	0.5-2 (1)	20-100 (40)	2.51
NW Europe	0.8-20 (6)	1-100 (3)	1-100 (80)	0.3-10 (1)	2-100 (100)	1.60
Barents Sea	3-20 (7)	0.1-1 (0.1)	0.1-1 (0.1)	1-4 (3)	10-100 (40)	2.68
BIFROST	0.2-4 (1)	0.2-2 (1)	0.1-100 (0.2)	1-10 (4)	10-100 (90)	4.06

2.5.3 Comparison with sea-level observations

In Fig. 2.7, selected sea-level observations are visually compared to predictions of the best multi-layer model for the Barents Sea, the NW European and the Scandinavian region, respectively. The red points indicate observations, the blue line the predictions for the best Barents Sea region model, the green line the predictions for the best model of the NW European region and the grey line the results for the Scandinavian region with its best model. The best multi-layer prediction for the Barents Sea model acceptably fit the observations of the three locations on Svalbard in the Barents Sea (blue circle, triangle and square). On the other hand, differences up to 15 m can be found between predictions and observations for the best multi-layer NW European region model, resulting from differences in the upper-mantle structure. Differences of up to 40 m 11,000 years ago can be found for the best multi-layer Scandinavian region model, caused by a different mantle structure with no indication of a low-viscosity zone.

The observations of the two locations on the British Isles (green circle and triangle) are acceptably fitted with the predictions of the best multi-layer NW European region model. For observations of the location Aberystwyth an good agreement is obtained for the two other best region models, caused by its

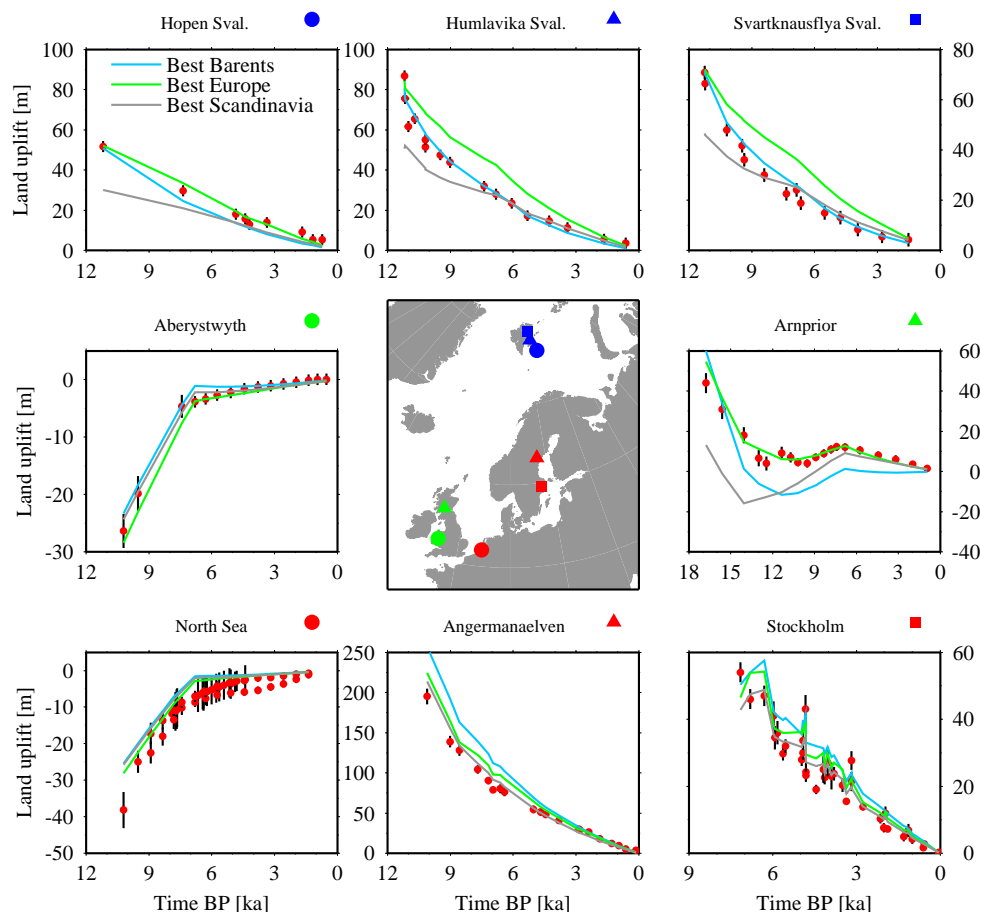


Figure 2.7: RSL observations (red dots with error bars) at selected locations on Europe compared with the predicted sea-level results from the best multi-layer model of the Barents Sea (blue lines), the NW European (green lines) and the Scandinavian region (grey lines). Symbols indicate the locations on the map.

distance to the former ice sheet. Here the eustatic sea-level change dominates the signal. In contrast, the observations of the location Arnprior show greater differences up to 60 m 17,000 years ago, a result of the different viscosity estimates.

The best multi-layer Scandinavian region model acceptably fits the observations of the two Swedish locations (red triangle and square). The two other best multi-layer models cause differences up to 50 m 10,000 years ago (see Ångermanaelven). Here, the best NW European model with no low-viscosity zone fits better than the best Barents Sea model including a low-viscosity zone.

No difference between the best region models can be found by comparison of observations of the North Sea location (red circle) with the results of the models. This is caused by the distance of this location to the former ice sheet, the eustatic sea-level change again controls the signal.

In Fig. 2.8, the radial component of the BIFROST GPS data [Johansson et al., 2002] are shown, together with a model prediction for the best NA solution, based on the viscosity profile shown in Fig. 2.6b. The predictions capture the uplift pattern well, both in amplitude and in shape. In general, differences between observations and predictions are below 1 mm/yr, with the two exceptions in Northern Finland and between Denmark and South Sweden.

2.6 Discussion

In this paper we have used two sets of observational data related to GIA: On the one hand, palaeo-shoreline data from Scandinavia, the Barents Sea, and NW Europe, covering the last deglaciation interval (21,400 years BP to present), and indicating a viscoelastic readjustment of the solid Earth after the disappearance of the Late Pleistocene ice sheets. On the other hand, crustal uplift data from Scandinavia collected by the BIFROST project, indicating an ongoing rebound of central Scandinavia.

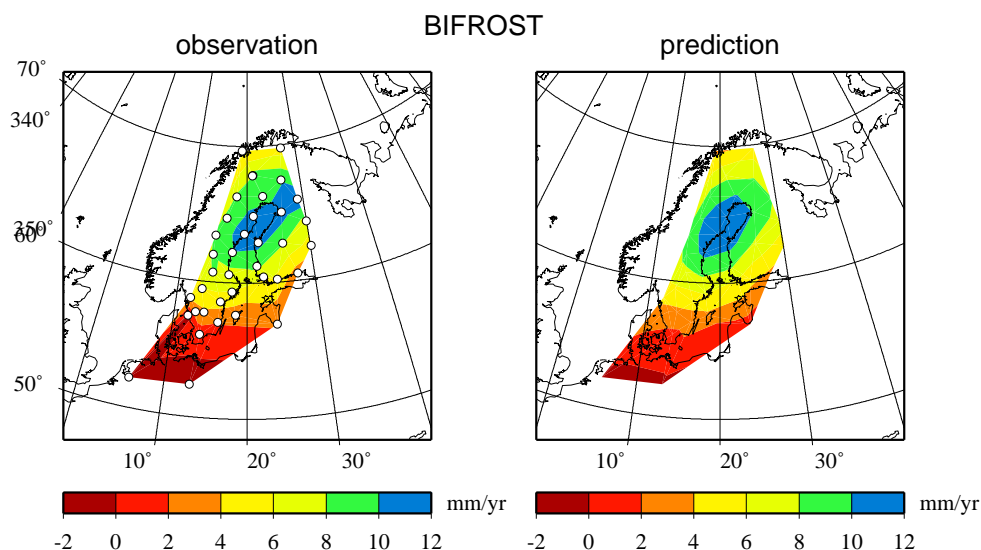


Figure 2.8: BIFROST uplift data (left) and model prediction from the best NA model (right). The BIFROST GPS stations are shown as circles. The difference between observations and predictions is smaller than 1 mm/yr almost everywhere.

We have used both data sets in an attempt to determine the radial viscosity variation in the Earth's mantle. In a first step, subregions of the shoreline data (Scandinavia, Europe, Barents Sea) are used to infer optimum values for lithospheric thickness and bulk upper- and lower-mantle viscosities. While lower-mantle viscosity is poorly constrained ($\eta_{LM} > 10^{22}$ Pa s), values for bulk upper-mantle viscosities are similar for all three subsets ($\eta_{UM} \sim 4 \times 10^{20}$ Pa s). Differences arise for the thickness of the lithosphere, with thicker values underneath Scandinavia ($H_l \sim 120$ km), and thinner values underneath the British Isles and the Barents Sea ($H_l \sim 60 - 70$ km). This lateral variability correlates with the thickening of the crust and lithosphere from the North Atlantic Mid-Ocean Ridge towards the Baltic Shield.

In a second step, we have refined the radial viscosity profiles with the Neighbourhood Algorithm, a global inverse procedure developed by Sambridge [1999a,b]. We therefore subdivided the upper mantle into five layers, in which viscosity can vary independently. This approach allows us to search for a low-viscosity asthenosphere, which has been proposed on the basis of RSL data from Scandinavia. The results from the NA inversion indicate a low-viscosity zone underneath the Barents Sea between 120 and 200 km depth, which is characterised by viscosities around $10^{19} - 10^{20}$ Pa s. The lower part of the upper mantle in these two regions becomes more viscous, with viscosities up to 10^{22} Pa s. However, underneath Scandinavia and NW Europe no evidence for a low-viscosity zone was found from the inversion of palaeo-shoreline data. Interestingly, the NA inversion of the BIFROST uplift data favours a thin low-viscosity layer between 160 - 200 km depth, which is in agreement with an earlier inference by Milne et al. [2004], but which is actually not resolved by the data.

Acknowledgements

We are grateful for numerous comments and suggestions by Detlef Wolf and an anonymous referee. Many thanks to Kurt Lambeck for providing the RSES ice model. We would also like to thank Malcolm Sambridge for permission to use the NA inversion package [Sambridge, 1999a,b, 1998, 2001]. The figures in this paper are drawn using the GMT graphics package [Wessel and Smith, 1991, 1998]. This research was funded by the DFG (research grant KA1723-1).